Alexandria Engineering Journal (2021) 60, 1955–1966

HOSTED BY

Alexandria University

Alexandria Engineering Journal

www.elsevier.com/locate/aej
www.sciencedirect.com

Evaluation of flow pattern recognition and void fraction measurement in two phase flow independent of oil pipeline's scale layer thickness

Mohammadmehdi Roshani [a,b], Giang T.T. Phan [a,b], Peshawa Jammal Muhammad Ali [c], Gholam Hossein Roshani [d], Robert Hanus [e], Trung Duong [a], Enrico Corniani [f,g,*], Ehsan Nazemi [h], El Mostafa Kalmoun [i]

[a] Institute of Fundamental and Applied Sciences, Duy Tan University, Ho Chi Minh City 700000, Viet Nam
[b] Faculty of Electrical – Electronic Engineering, Duy Tan University, Da Nang 550000, Viet Nam
[c] Department of Software Engineering, Faculty of Engineering, Koya University, Koya KOY45, Kurdistan Region F.R. Iraq
[d] Electrical Engineering Department, Kermanshah University of Technology, Kermanshah, Iran
[e] Rzeszów University of Technology, Faculty of Electrical and Computer Engineering, Rzeszów, Poland
[f] Division of Nuclear Physics, Advanced Institute of Materials Science, Ton Duc Thang University, Ho Chi Minh City, Viet Nam
[g] Faculty of Applied Sciences, Ton Duc Thang University, Ho Chi Minh City, Viet Nam
[h] Imec-Vision Lab, Department of Physics, University of Antwerp, Antwerp, Belgium
[i] Department of Mathematics, Statistics and Physics, College of Arts and Sciences, Qatar University, Qatar

Received 29 June 2020; revised 12 October 2020; accepted 30 November 2020
Available online 11 December 2020

KEYWORDS

Flow pattern;
Scale layer;
Oil pipeline;
Support vector machine;
Multi-layer perceptron

Abstract The main objective of the present research is to combine the effect of scale thickness on the flow pattern and characteristics of two-phase flow that is used in oil industry. In this regard, an intelligent nondestructive technique based on combination of gamma radiation attenuation and artificial intelligence is proposed to determine the type of flow pattern and gas volume percentage in two phase flow independent of petroleum pipeline's scale layer thickness. The proposed system includes a dual energy gamma source, composed of Barium-133 and Cesium-137 radioisotopes, and two sodium iodide detectors for recording the transmitted and scattered photons. Support Vector Machine was implemented for regime identification and Multi-Layer Perceptron with Levenberg Marquardt algorithm was utilized for void fraction prediction. Total count in the scattering detector and counts under photo peaks of Barium-133 and Cesium-137 were assigned as the inputs of networks. The results show the ability of presented system to identify the annular regime and measure the void fraction independent of petroleum pipeline's scale layer thickness.

* Corresponding author.
E-mail address: enrico.corniani@tdtu.edu.vn (E. Corniani).
Peer review under responsibility of Faculty of Engineering, Alexandria University.

https://doi.org/10.1016/j.aej.2020.11.043

1. Introduction

In petroleum industry, quantitative measuring of the gas and oil components are essential. With sufficient information on the gas and oil phase's volume fractions, the separating process could be optimized. Also, it is necessary to recognize the type of flow pattern in the transportation process and also determine the volume fractions of the gas and oil phases, because these two flow characteristics are directly related to the process's economics. Type of flow regime can affect the separating process's efficiency, whilst each component's volume fraction provides indication as to whether the drilling process must be continued or stopped. Lots of technique such as hydrostatic, ultrasonic, hydrometric, and gamma radiation techniques have been applied for determining flow regime and volume fraction of two-phase flow. Among the mentioned techniques, gamma radiation based technique has attracted more attention because of its advantages such as being nondestructive, non-intrusive, applicable in harsh conditions, and etc.

In recent decades, numerous studies have been done on determining flow regime and volume fractions of multiphase flows using gamma radiation based technique. In 1999, Abro and his colleagues presented a multi-beam radiation technique to recognize flow patterns of a two phase flow inside a small diameter pipe [1]. They used EGS4 software package to simulate a detection system included one americium-241 radioisotope source and three detectors with orientations of 140°, 154° and 180° in respect to the radioisotope source. They simulated three flow regimes of homogeneous, stratified and annular with void fraction percentages from 0 up to 100%. Using artificial neural network (ANN), they could identify all the flow patterns and forecast the void fraction percentage with an error of 3%. In 2015, Faghihi and his colleagues carried out an experimental investigation to identify flow pattern's type of a modelled two-phase flow [2]. They implemented some polyethylene phantoms to model various flow regimes and void fraction percentages in static conditions. Their experimental arrangement consisted of two sodium iodide (NaI) crystal detectors and one Cesium-137 radioisotope. Using a correlation method, they succeeded to identify type of flow regimes. In 2017, G.H. Roshani et al. presented a new method to identify flow pattern and forecast the void fraction in two phase flows without any dependency to changes of liquid phase density [3]. The methodology included a dual modality gamma radiation technique, consisted of one Cesium-137 source and three sodium iodide detectors, combined with multi-layer perceptron (MLP) neural network. They utilized two detectors for recording the scattered and transmitted photons. Applying four ANNs, they succeeded to identify all the three flow patterns and determine void fraction without any dependency to liquid phase density changes. In 2020, Sattari et al. tried to improve measurement precision of a simple two-phase flowmeter consisted of a Cesium-137 source and one sodium iodide detector [4]. At first they applied Savitzky-Golay filter on the extracted photon energy spectrum from detector to eliminate high-frequency noises related to uncertainty of obtained calculations in the MCNPX code. Then, they extracted seven features of average value, variance, skewness, kurtosis, waveform length, absolute value of the summation of the root (ASM), and absolute value of the summation of square root (ASS) in time domain from the denoised spectrum and assigned them as inputs of neural network. Using this method, they succeeded to recognize the type of flow regimes and predict void fraction with a relative error of less than 1.11. More related studies in the field of radiation multiphase flowmeters as well as application of artificial intelligence in engineering fields can be found in references [5–21].

Performance of radiation-based flow meters depends powerfully on the different parameters. For example, changes in fluid density, temperature or pressure can cause errors in determination of the volume fractions. A conventional solution in order to solve this problem is recalibration. Usage of ANN for solving this problem is an almost new method which is used in many studies. In [22], a method was proposed in order to determinate the void fraction in two-phase flow independent of density changes using ANN. In [23], it was shown that a combination of ANN and gamma-ray densitometer can be used to measure the volume fractions independent of density changes in multiphase flows.

Conventional gamma radiation based two-phase flowmeters can just work properly when the flow characteristics such as flow regime and volume fractions of component change inside the pipe. But sometimes, minerals are gradually deposited inside the oil pipelines and leads to formation of a scale layer which can consequently decrease precision and performance of gamma radiation based two-phase flowmeters. A sample of scale layer formed in an oil pipeline is shown in Fig. 1. As described above, recent studies concentrated on determining flow pattern and gas volume percentage of two phase flows without considering scale layer inside the pipe. On the other hand, some researchers just focused on measuring the scale thickness in oil pipelines using radiation based techniques regardless of flowing fluid inside them [24–29]. The main objective of the present research is to combine the effect of scale thickness on the flow pattern and characteristics of two-phase flow that is used in oil industry. In this regard, a

Fig. 1 A sample of scale layer formed in an oil pipeline [25].

dual energy gamma radiation based system is proposed to determine the type of flow pattern and estimate void fraction in two phase flow independent of petroleum pipeline's scale layer thickness.

2. Materials and methods

2.1. Detection system

Version X of Monte Carlo N Particle code (MCNPX) [30] was used in this study to model the detection system. The proposed detection system includes a dual energy gamma source, composed of Barium-133 and Cesium-137 radioisotopes, and two sodium iodide. A steel pipe that two phase flow and scale layer are modeled inside, was also located between radioactive source and detectors. Schematic view of simulated detection system is shown in Fig. 2. In this figure, stratified flow regime modelled inside the steel pipe has been shown as an example. The proposed system can be divided into three main parts that will be described in the following.

2.1.1. Radiation source

The radiation source includes Barium-133 and esium-137 radioisotopes which emit gamma radiation with energies of 0.356 and 0.662 MeV, respectively. A disk source was defined to model the radiation source. Source information (SI) and source probability (SP) cards in source definition (SDEF) section of MCNPX input file were used to define Barium-133 and Cesium-137 radioisotopes. The gamma ray emission probability from both radioisotopes was considered equal. The disk source was put inside a lead shield in order to collimate the radiation beam toward the transmission detector.

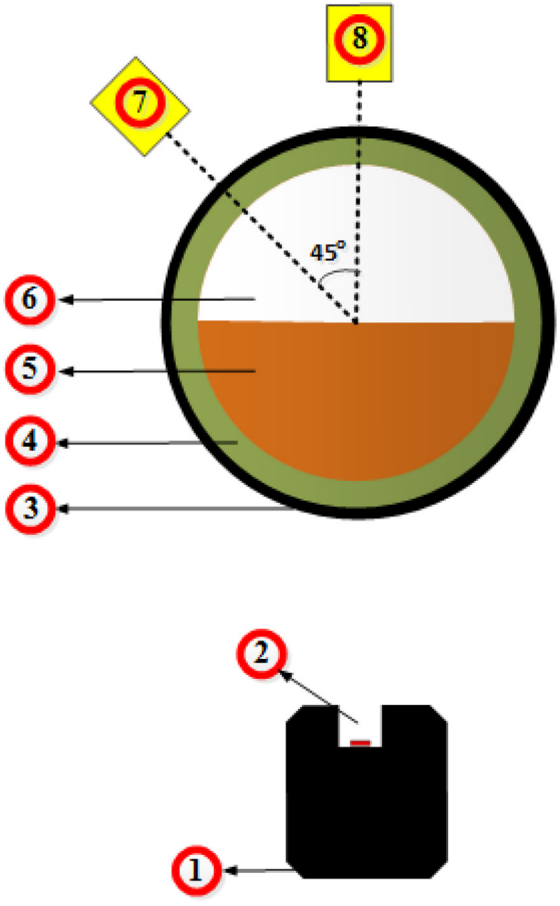

Fig. 2 Simulated detection system:1-Shield, 2-Dual energy source, 3-Steel pipe, 4-Scale layer, 5-Liquid phase, 6-Gas phase, 7-Scattering detector, 8-Transmission detector.

2.1.2. Detector

In this investigation, two 25.4 mm × 25.4 mm sodium iodide detectors were utilized in order to record the transmitted and scattered photons. The detector used for recording the transmitted photons was diametrically located in front of radiation source and the other detector was located at the angle of 45° respect to the connecting line of pipe's center to transmission detector.

In order to register photon spectrum in both detectors, pulse height tally (Tally F8) was used in the simulations. In order to take the photon spectrum broadening into account with the aim of making the simulated detector responses closer to the experimental ones, Gaussian energy broadening (GEB) option was also implemented. At the first step, FWHMs of the full energy peak for some different energies were calculated via experiments and then were inserted into the "FT8 GEB" card. The mentioned card has 3 parameters, called "a", "b" and "c" that should be determined on the basis of equation (1) [30]:

$$FWHM = a + b\sqrt{E + cE^2} \tag{1}$$

In a former research, an experimental setup that was consisted of a 1 in. × 1 in. NaI detector and 3 radioactive gamma emitter sources (^{241}Am, ^{137}Cs and ^{60}Co), was developed to measure the necessary constant parameters [31]. The obtained FWHMs are shown in table 1.

At the final step, the obtained FWHMs shown in table 1 were plotted against energy and then a curve on the basis of equation (1) was fitted to the data. Utilizing the explained approach, "a", "b" and "c" parameters were determined 1.09 × 10^{-2} (MeV), 6.96 × 10^{-2} ($MeV^{0.5}$) and 2.26 × 10^{-2} (MeV^{-1}), respectively. The calculated parameters were inserted in input file to take the energy broadening of photon spectrum into account in the modelled sodium iodide crystal detector.

In Fig. 3, some recorded spectra in both detectors for three flow regimes with scale thickness of 0.5 cm and void fraction of 40% are shown as an example. In transmission detector, counts under photo peaks of Barium-133 and Cesium-137 were extracted from the recorded photon energy spectrum. In the scattering detector, count under the entire of spectrum (total count) was extracted. The mentioned three extracted counts from the recorded photon energy spectra in both detectors were applied for training and testing of the neural network. It is worth mentioning that the STOP card with a value of 0.01 was used in the input file of MCNP code to reduce the effect of Monte Carlo statistical errors on the calculations.

2.1.3. Scale layer and two phase flow modelling

A pipe made of steel with external and internal diameters of 21 cm and 20 cm respectively was considered as the main pipe in the simulations. In the interior wall of the pipe, a symmetric annular layer made of Barium Sulfate (BaSO4) with different

Table 1 The obtained photo peak's FWHM for various energies.

Energy (eV)	5.95×10^4	6.62×10^5	1.17×10^6	1.33×10^6
FWHM (eV)	6.1×10^3	4.55×10^4	6.71×10^4	6.94×10^4

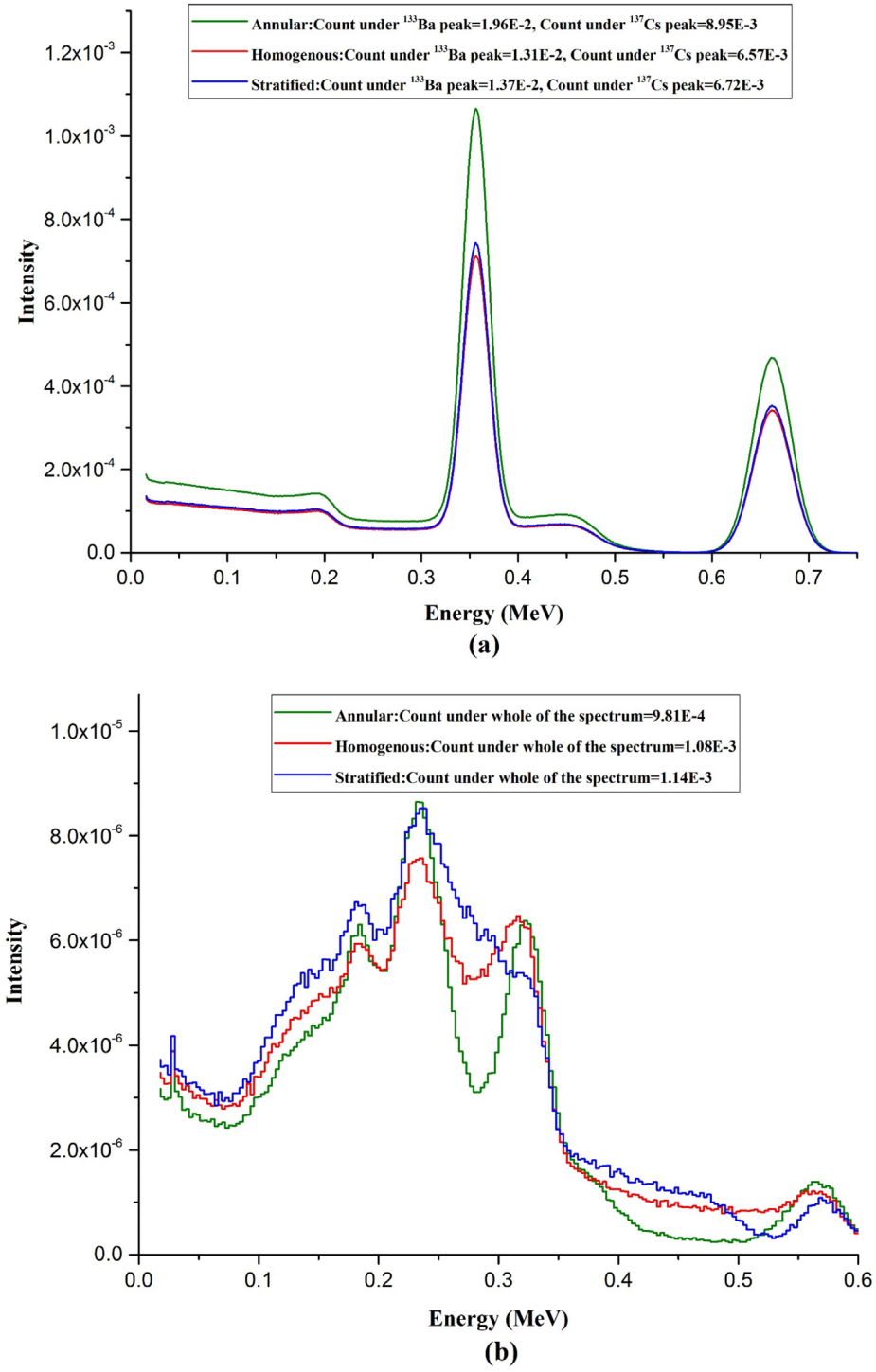

Fig. 3 Recorded spectra for three flow regimes with scale thickness of 0.5 cm and void fraction of 40% in: a) transmission detector b) scattering detector.

thicknesses was considered as the scale. A gas–liquid two phase flow with various flow regimes and gas volume fractions was also modelled inside the pipe. Specifications of modelled scale layer and two-phase flow inside the main pipe are indicated in table 2 and Fig. 4.

2.2. Regime identification using SVM

For regime identifying, Support Vector Machine (SVM) as a very effective tool for classification was used [32]. SVM is a binary classification tool which takes labeled data from two classes as inputs [33–34]. This machine after training can classify new unlabeled data into two specified classes. Like other machine learning techniques, there are two essential steps in the usage of SVM namely training and testing. The testing step is used to validate the learned machine.

The SVM has many benefits in solving problems with small sample size. Also, it has many advantages in solving problems of high dimensional and nonlinear pattern recognition. Furthermore, this strong classifier has a high reliability. SVM classifies data on the basis that it may or may not be linearly separable in its domain of origin. If the data in its original domain is linearly separable, the simple linear SVM is utilized and, if the data can not be distinguished, it should be projected into a higher-dimensional space using appropriate kernel function. The data would be linearly distinguishable in a higher-dimensional space. The performance of SVM classifier is strongly dependent on the selection of the kernel functions. In this study, Linear, Polynomial, Quadratic, Multi-Layer Perceptron and Radial Basis Function were tested as kernel functions and the best one was selected.

Table 2 Specifications of modelled scale layer and two-phase flow inside the main pipe.

Specification	Value/Name
Type of material used for scale layer	BaSO4
Thickness range of scale layer	0–4 cm
Step of scale layer's thickness	0.5 cm
Number of phases	2
Type of material used for liquid phase	Gasoil
Type of material used for gas phase	Air
Density of material used for liquid phase	826 kg/m^3
Density of material used for gas phase	1.25 kg/m^3
Number of flow regimes	3
Type of flow regimes	Stratified, Annular, Homogenous
Range of void fraction percentages	10–85%
Step of void fraction percentage	15%
Total number of performed simulations	9 scale thicknesses × 3 flow regimes × 6 void fractions = 162

The performance of a SVM classifier which is binary classifier is obtained using the sensitivity, specificity and accuracy indexes [35]:

$$\text{Sensitivity} = TP / (TP + FN) \quad (2)$$

$$\text{Specificity} = TN / (TN + FP) \quad (3)$$

$$\text{Accuracy} = (TP + TN) / (TP + TN + FP + FN) \quad (4)$$

where TP, FN, TN and FP are the number of true positive, false negative, true negative and false positive classified cases, respectively. The SVM classification in TP and TN is correct but in FP, SVM labels a case as positive if it is negative and in FN, SVM labels a case as negative if it is positive.

In our proposed method, in the first step it was attempted to classify the annular regime from the other both regimes. SVM is binary classifier and this is the reason of this method. Therefore the annular regime was considered 1 and other regimes (homogenous and stratified) were considered −1. In the last step it was attempted to separate the homogenous regime from stratified regime. Therefore the homogenous regime was considered 1 and stratified regime was considered −1. In this regard, two different procedures were performed: "2 inputs" and "3 inputs". In the first procedure, 2 inputs were considered for the SVM: total count in the scattering detector and counts under photo peak of Cesium-137 and in the second one, 3 inputs were considered: total count in the scattering detector and counts under photo peaks of Cesium-137 and Barium-133. The results of this method in order to identify the regime are given in the results and discussion section.

2.3. Void fraction measuring using MLP

For void fraction measuring, Multi-Layer Perceptron (MLP) as a very powerful tool for regression and prediction was used. Also, for the MLP training process, Levenberg Marquardt (LM) algorithm was used. The LM algorithm which is the

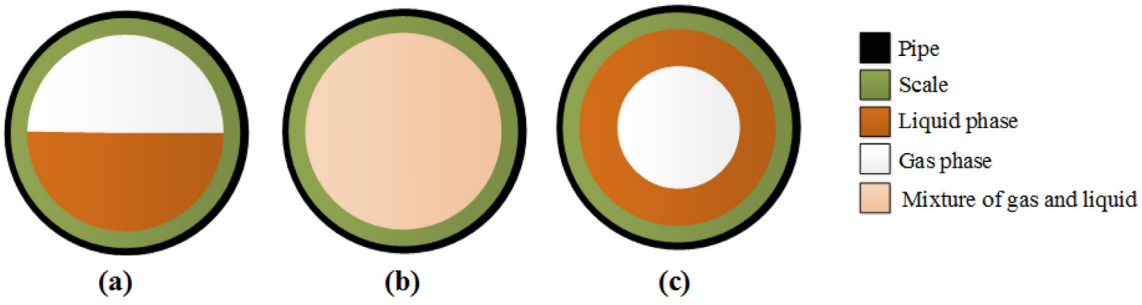

Fig. 4 Modelled scale layer and two-phase flow regimes inside the main pipe: a) Stratified regime, b) Homogenous regime, c) Annular regime.

most widely used optimization algorithm has been obtained by combination of Gauss-Newton and gradient descent and method.

MLP can be used to linear or non-linear mapping between an N-dimensional input vectors to an $M-$dimensional output vectors. Back-propagation which is a supervised learning technique is used for MLP training. MLP has three layers: input layer, hidden layer and output layer. Each layer consists of several neurons that use linear or non-linear activation functions. The neurons in every layer have direct connections to the neurons of next layer. These connections make weights and biases matrix. Its non-linear activation functions and multiple layers distinguish MLP from a linear perceptron. MLP can distinguish data that is not linearly separable. There are several optimization algorithms for training the MLP and obtaining the weights and biases. LM algorithm which is a well-known opti-

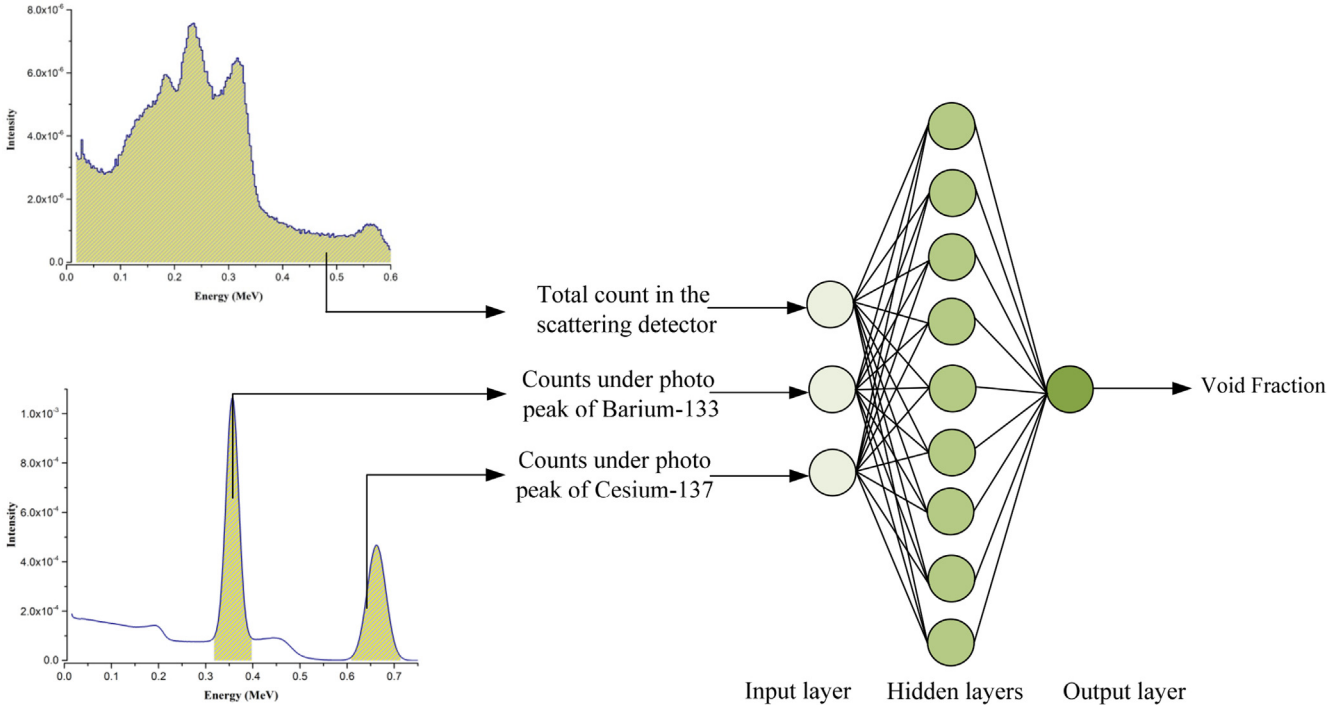

Fig. 5 Architecture of proposed network in order to measure the void fraction.

Table 3 Classification results for separating annular regime from other regimes.

Binary classes	Number of data for testing the performance	Number of inputs	Kernel Used	TP	TN	FP	FN	Sensitivity	Specificity	Accuracy
Annular = +1	48	2 (total count in the scattering detector and counts under photo peak of Cesium-137)	Linear	5	27	5	11	0.312	0.843	0.666
			Polynomial (order = 3)	13	22	10	3	0.812	0.687	0.729
Other Regimes = -1			Quadratic	9	27	5	7	0.562	0.843	0.750
			Multi-Layer Perceptron	4	24	8	12	0.250	0.750	0.583
			Radial Basis Function (sigma = 0.2)	14	26	6	2	0.875	0.812	0.833
		3 (total count in the scattering detector and counts under photo peaks of Cesium-137 and Barium-133)	Linear	5	27	5	11	0.312	0.843	0.666
			Polynomial (order = 4)	15	27	5	1	0.937	0.843	0.875
			Quadratic	10	25	7	6	0.625	0.781	0.729
			Multi-Layer Perceptron	4	26	6	12	0.250	0.812	0.625
			Radial Basis Function (sigma = 0.2)	12	27	5	4	0.750	0.843	0.812

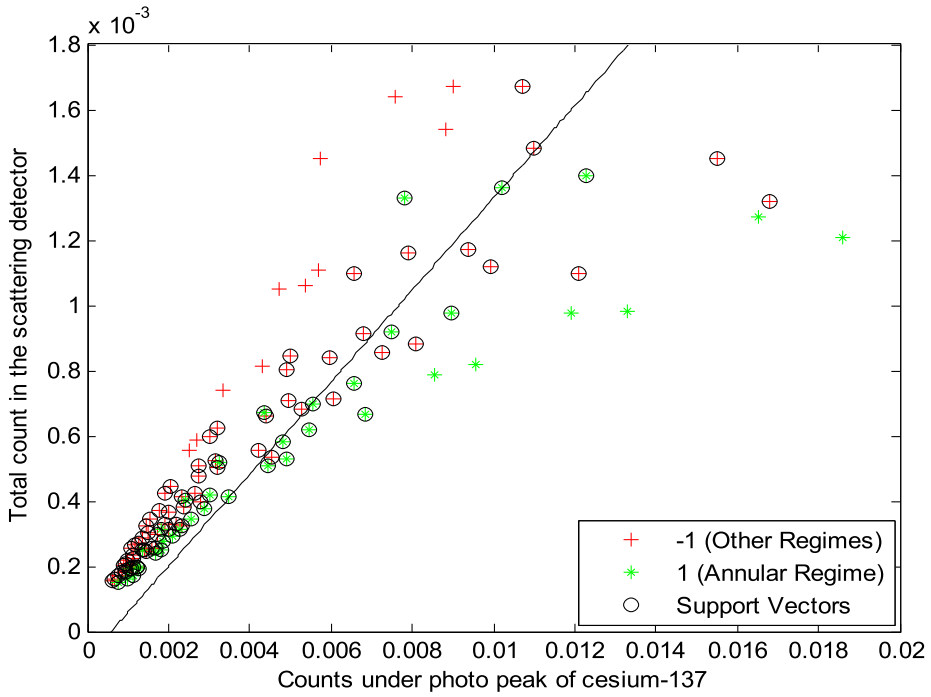

(a)

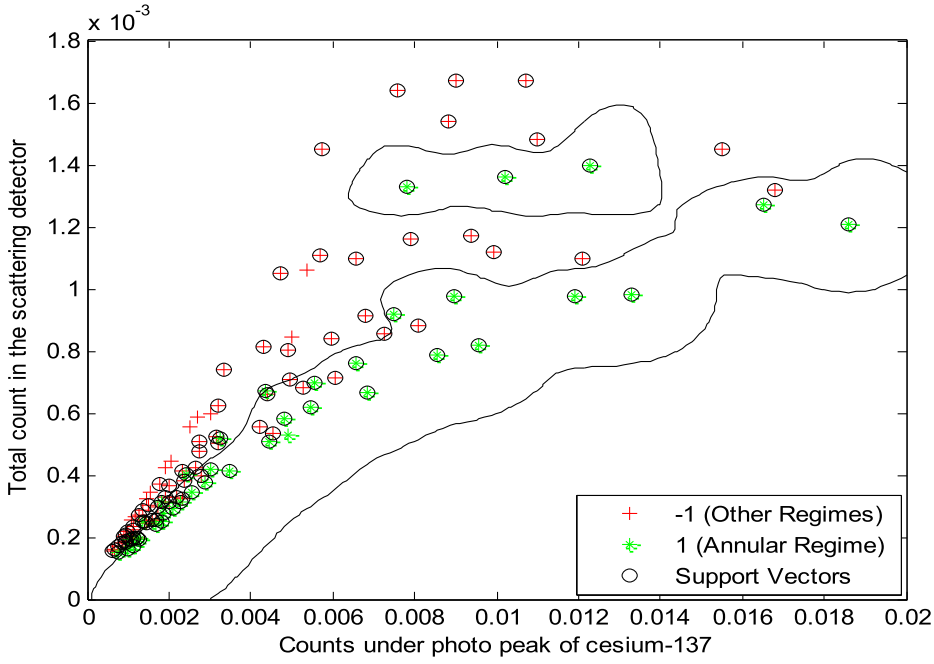

(b)

Fig. 6 Classification of SVM using 2 inputs a) linear kernel b) Radial Basis Function with sigma = 0.2 as kernel function.

mization algorithm for obtaining weights and biases matrix is obtained by combination of gradient descent and Gauss-Newton. This optimization algorithm outperforms gradient descent and other methods of conjugating gradient in a wide range of problems [36].

In the usage of MLP like other models, there are two essential steps namely training and testing. The testing step is used to check the learned machine.

In this study, a MLP-LM network with three inputs and one output was considered. Total count in the scattering detec-

Table 4 Classification results for separating homogenous regime from stratified regime.

Binary classes	Number of data for testing the performance	Number of inputs	Kernel Used	TP	TN	FP	FN	Sensitivity	Specificity	Accuracy
Homogenous = +1	32	2 (total count in the scattering detector and counts under photo peak of Cesium-137)	Linear	9	11	4	8	0.529	0.733	0.625
			Polynomial (order = 3)	9	6	9	8	0.529	0.400	0.468
			Quadratic	9	6	9	8	0.529	0.400	0.468
Stratified = -1			Multi-Layer Perceptron	4	11	4	13	0.235	0.733	0.468
			Radial Basis Function (sigma = 0.2)	8	5	10	9	0.470	0.333	0.406
		3 (total count in the scattering detector and counts under photo peaks of Cesium-137 and Barium-133)	Linear	11	8	7	6	0.647	0.533	0.593
			Polynomial (order = 4)	7	7	8	10	0.411	0.466	0.437
			Quadratic	9	5	10	8	0.529	0.333	0.437
			Multi-Layer Perceptron	4	13	2	13	0.235	0.866	0.531
			Radial Basis Function (sigma = 0.2)	5	4	11	12	0.294	0.266	0.281

tor and counts under photo peaks of Barium-133 and Cesium-137 were assigned as the inputs of MLP-LM and the void fraction was considered as output. The architecture of proposed network to measure void fraction is illustrated in Fig. 5.

The performance of a MLP model is obtained using the Mean Absolute Error (MAE), Mean Relative Error percentage (MRE %) and Root Mean Square Error (RMSE) :

$$MAE = \frac{1}{N}\sum_{i=1}^{Z}|X_i(Actual) - X_i(Measured)| \quad (5)$$

$$MRE\% = 100 \times \frac{1}{N}\sum_{i=1}^{N}\left|\frac{X_i(Actual) - X_i(Measured)}{X_i(Actual)}\right| \quad (6)$$

$$RMSE = \left[\frac{\sum_{i=1}^{N}(X_i(Actual) - X_i(Measured))^2}{N}\right]^{0.5} \quad (7)$$

As can be mentioned previously, in the MCNP simulations, 162 different cases in different conditions were simulated. 70% of data (114 cases) were used for training the model and 30% (48 cases) were used for testing the efficiency of presented MLP-LM model. For finding the optimized network architecture, different structures were tested in different nested loops based on below algorithm:

1) *The initial values were set.*
2) *Some nested loops were formed.*
3) *The errors were defined.*
4) *Various epochs and different number of hidden layers and neurons in each layer were tested.*
5) *The efficiency of each structure was obtained using the defined errors.*
6) *The best artificial neural network with lowest errors was saved.*

The best structure had one hidden layer with 9 neurons and number of epochs was 680. The activation functions of input, hidden and output layers were "purelin", "tansig" and "purelin", respectively. The results of this method in order to measure the void fraction are given in the results and discussion section.

3. Results and discussion

The results of regime identification (classification problem) and identifying the annular regime from other both regimes were tabulated in Table 3 and a typical classification in "2 inputs" procedure was shown in Fig. 6.

As can be concluded from the Fig. 6 and Table 3, the learned machine can identify the annular regime with the accuracy of 87% which is not very high precision. As can be mentioned previously, identifying the annular regime is the first step. In the next step it was attempted to classify the homogenous regime from stratified regime. Therefore the homogenous regime was considered 1 and stratified regime was considered −1. The results were tabulated in Table 4 and a typical classification in "2 inputs" procedure is shown in Fig. 7.

As can be concluded from the Fig. 7 and Table 4, the learned machine can't identify the flow regime when the regime is homogenous or stratified. These regimes have similar behavior and there are a lot of overlaps for different cases with different void fractions. As mentioned in Table 4, there are two different inputs for best SVM classifier: total count in the scattering detector and counts under photo peak of Cesium-137. The values of these inputs are similar in the cases of homogeneous and stratified regimes. In fact, the classifier system should distinguish different regimes with similar input features. Obviously, this system cannot distinguish the mentioned regimes.

In future studies, it could be investigated how to improve the accuracy of this system. For example, using different detec-

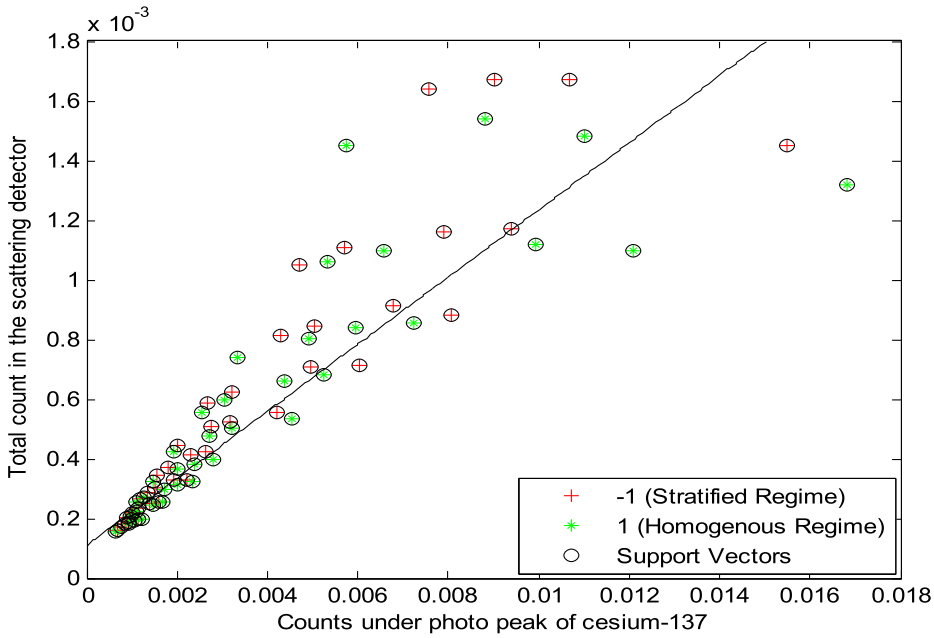

(a)

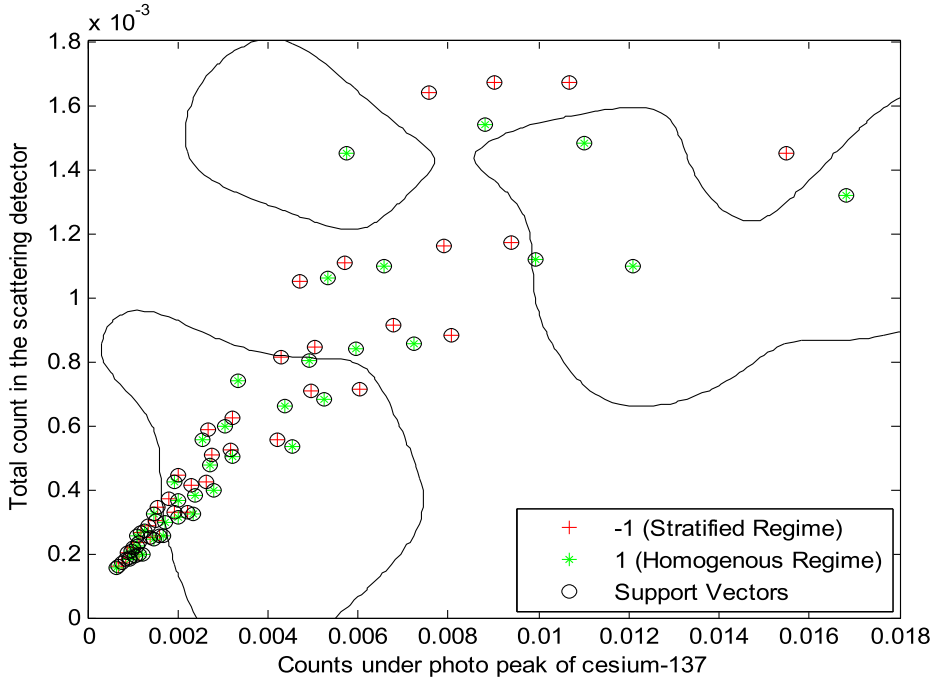

(b)

Fig. 7 Classification of SVM using 2 inputs a) linear kernel b) Radial Basis Function with sigma = 0.4 as kernel function .

tion geometries or using different types of radiation sources (X-ray instead of single energy radioisotopes) may resolve this problem. Perhaps the problem could be solved by different time-domain, frequency-domain or time–frequency feature extraction from the inputs spectra.

In the void fraction measuring problem, differences between real data and predicted data by proposed MLP-LM model was obtained and shown in Fig. 8. The appropriate agreement between actual and measured data is clearly found from these regression diagrams. In Table. 5, the inputs, real outputs and measured outputs were tabulated for test data set.

The obtained errors for suggested ANN structure were tabulated in Table 6. The low error for measuring the void fraction shows the good performance of presented method.

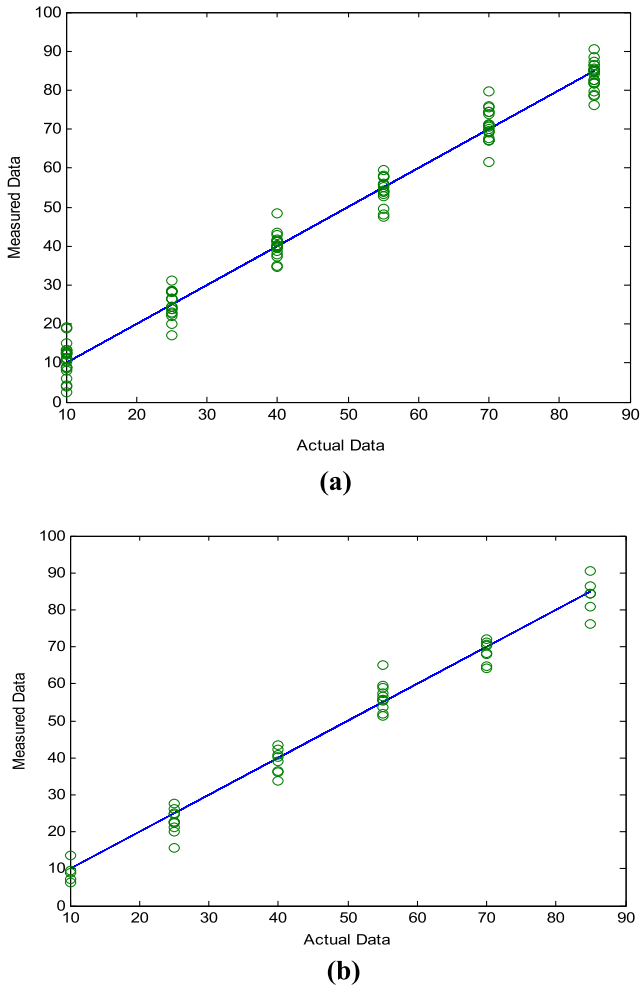

Fig. 8 Regression diagrams of real and measured results for a) train data b) test data.

In this paper, the application of the proposed system was proved. However, it could be improved by usage of different detection geometries, different types of radiation sources (X-ray instead of single energy radioisotopes) or different soft computing methods. Also, the present study could be continued with usage of experimental data from appropriate test loop in order to be employed in different industries.

4. Conclusions

In this paper, a novel radiation based system in order to meter two-phase flow was presented which can identify the annular regime and measure the void fraction independent of petroleum pipeline's scale layer thickness. The problem of this study was divided into two sections: classification and regression. For the first problem, it was attempted to classify the annular regime from other regimes. SVM as a very powerful binary classifier with different kernel functions was used. Linear, Polynomial, Quadratic, Multi-Layer Perceptron and Radial Basis Function were used as kernel functions. The learned machine can identify the annular regime with the accuracy of 87%. Then, it was attempted to separate the homogenous regime from stratified regime. The trained system can't identify the flow regime when the regime is homogenous or stratified because of similar behavior and several overlaps for different cases with different void fractions. For the second problem, it was attempted to determine the gas volume percentage independent of scale thickness. MLP-LM as a powerful tool was used. The proposed architecture for MLP-LM had one hidden layer with 9 neurons and number of epochs was 680. The activation functions of input, hidden and output layers were purelin, tansig and purelin, respectively. Good performance of presented method for measuring the gas volume fraction was proved with MAE of less than 2.82.

Table 5 The test data with measured values.

Data Number	Flow Regime	Total count in the scattering detector	Counts under photo peak of Cesium-137	Counts under photo peak of Barium-133	Scale Layer Thickness	Actual Void Fraction	Measured Void Fraction
1	Annular	3.96E-02	1.44E-02	1.35E-03	0	55	55.37
2	Annular	1.14E-02	5.81E-03	9.04E-04	0.5	10	6.38
3	Annular	2.37E-02	1.04E-02	9.79E-04	0.5	55	51.81
4	Annular	1.41E-02	7.55E-03	7.73E-04	1	55	56.59
5	Annular	5.87E-03	4.07E-03	5.36E-04	1.5	25	20.11
6	Annular	9.83E-03	6.16E-03	6.43E-04	1.5	70	68.12
7	Annular	4.38E-03	3.50E-03	4.49E-04	2	40	40.84
8	Annular	5.13E-03	3.96E-03	4.76E-04	2	55	53.76
9	Annular	2.26E-03	2.23E-03	3.21E-04	2.5	25	15.54
10	Annular	3.54E-03	3.19E-03	3.96E-04	2.5	70	71.93
11	Annular	1.41E-03	1.66E-03	2.55E-04	3	25	24.97
12	Annular	2.37E-03	2.50E-03	3.29E-04	3	85	86.43
13	Annular	1.03E-03	1.38E-03	2.09E-04	3.5	40	40.16
14	Annular	1.17E-03	1.53E-03	2.25E-04	3.5	55	57.57
15	Annular	5.65E-04	8.98E-04	1.54E-04	4	25	26.30
16	Annular	8.01E-04	1.20E-03	1.83E-04	4	70	70.66
17	Homogenous	1.62E-02	7.11E-03	1.51E-03	0	25	22.78
18	Homogenous	3.68E-02	1.36E-02	1.45E-03	0	70	64.77

Table 5 (*continued*)

Data Number	Flow Regime	Total count in the scattering detector	Counts under photo peak of Cesium-137	Counts under photo peak of Barium-133	Scale Layer Thickness	Actual Void Fraction	Measured Void Fraction
19	Homogenous	7.82E-03	4.38E-03	9.90E-04	0.5	10	8.83
20	Homogenous	1.69E-02	8.10E-03	1.14E-03	0.5	55	64.94
21	Homogenous	6.37E-03	4.03E-03	7.77E-04	1	25	22.52
22	Homogenous	1.70E-02	8.77E-03	8.61E-04	1	85	90.51
23	Homogenous	5.07E-03	3.64E-03	6.27E-04	1.5	40	36.37
24	Homogenous	1.01E-02	6.30E-03	6.90E-04	1.5	85	84.47
25	Homogenous	2.55E-03	2.29E-03	4.51E-04	2	25	24.65
26	Homogenous	4.87E-03	3.83E-03	5.22E-04	2	70	70.40
27	Homogenous	1.63E-03	1.72E-03	3.48E-04	2.5	25	22.26
28	Homogenous	3.63E-03	3.26E-03	4.10E-04	2.5	85	80.93
29	Homogenous	1.25E-03	1.49E-03	2.83E-04	3	40	33.85
30	Homogenous	5.63E-04	8.32E-04	1.97E-04	3.5	10	7.18
31	Homogenous	9.43E-04	1.28E-03	2.33E-04	3.5	55	55.69
32	Homogenous	4.33E-04	7.22E-04	1.62E-04	4	25	21.15
33	Homogenous	5.07E-04	8.20E-04	1.73E-04	4	40	36.02
34	Stratified	1.37E-02	6.17E-03	1.59E-03	0	10	9.60
35	Stratified	3.46E-02	1.28E-02	1.62E-03	0	70	68.24
36	Stratified	1.37E-02	6.72E-03	1.16E-03	0.5	40	38.92
37	Stratified	2.68E-02	1.14E-02	1.12E-03	0.5	85	76.23
38	Stratified	5.48E-03	3.57E-03	7.70E-04	1	10	13.54
39	Stratified	1.03E-02	5.82E-03	8.83E-04	1	55	51.21
40	Stratified	5.21E-03	3.73E-03	6.57E-04	1.5	40	42.27
41	Stratified	6.25E-03	4.30E-03	6.89E-04	1.5	55	55.59
42	Stratified	2.71E-03	2.39E-03	4.77E-04	2	25	27.67
43	Stratified	4.54E-03	3.63E-03	5.51E-04	2	70	71.22
44	Stratified	2.02E-03	2.04E-03	3.89E-04	2.5	40	43.30
45	Stratified	3.33E-03	3.05E-03	4.30E-04	2.5	85	84.23
46	Stratified	1.48E-03	1.71E-03	3.21E-04	3	55	58.80
47	Stratified	9.27E-04	1.26E-03	2.44E-04	3.5	55	59.54
48	Stratified	6.62E-04	1.02E-03	1.93E-04	4	70	64.28

Table 6 Obtained errors for suggested ANN structure.

Output	MRE		RMSE		MAE	
	Train	Test	Train	Test	Train	Test
Void fraction	0.46	1.01	3.67	3.66	2.79	2.81

Declaration of Competing Interest

The authors declare that they have no known competing financial interests or personal relationships that could have appeared to influence the work reported in this paper.

References

[1] E. Abro, V.A. Khoryakov, G.A. Johansen, Determination of Void Fraction and Flow Regime Using a Neural Network Trained on Simulated Data Based on Gamma-Ray Densitometry, Meas. Sci. Technol. 10 (1999) 619–630.

[2] R. Faghihi, M. Nematollahi, A. Erfaninia, M. Adineh, Void fraction measurement in modeled two-phase flow inside a vertical pipe by using polyethylene phantoms, Int. J. Hydrogen Energy 40 (2015) 15206–15212.

[3] G.H. Roshani, E. Nazemi, M.M. Roshani, Identification of flow regime and estimation of volume fraction independent of liquid phase density in gas-liquid two-phase flow, Prog. Nucl. Energy 98 (2017) 29–37.

[4] M.A. Sattari, G.H. Roshani, R. Hanus, Improving the structure of two-phase flow meter using feature extraction and GMDH neural network, Radiat. Phys. Chem. 171 (2020) 108725.

[5] V. Mosorov, Improving the accuracy of single radioactive particle technique for flow velocity measurements, Flow Meas. Instrum. 66 (2019) 150–156.

[6] G.H. Roshani, E. Nazemi, S.A.H. Feghhi, S. Setayeshi, Flow regime identification and void fraction prediction in two-phase flows based on gamma ray attenuation, Measurement 62 (2015) 25–32.

[7] E. Nazemi, G.H. Roshani, S.A.H. Feghhi, R. Gholipour Peyvandi, S. Setayeshi, Precise Void Fraction Measurement in Two-Phase Flows Independent of the Flow Regime using gamma-ray attenuation, Nuclear, Eng. Technol. 48 (2016) 64–71.

[8] A. Karami, G.H. Roshani, A. Salehizadeh, E. Nazemi, The fuzzy logic application in volume fractions prediction of the annular three-phase flows, J. Nondestr. Eval. 36 (2017) 35.

[9] M. Roshani, M.A. Sattari, P.J.M. Ali, et al, Application of GMDH neural network technique to improve measuring precision of a simplified photon attenuation based two-phase flowmeter, Flow Meas. Instrum. 75 (2020) 101804.

[10] C. Sætre, S.A. Tjugum, G.A. Johansen, Tomographic segmentation in multiphase flow measurement, Radiat. Phys. Chem. 95 (2014) 420–423.
[11] G.H. Roshani, E. Nazemi, M.M. Roshani, A novel method for flow pattern identification in unstable operational conditions using gamma ray and radial basis function, Appl. Radiat. Isot. 123 (2017) 60–68.
[12] A. Karami, G.H. Roshani, A. Khazaei, E. Nazemi, M. Fallahi, Investigation of different sources in order to optimize the nuclear metering system of gas–oil–water annular flows, Neural Comput. Appl. 32 (2020) 3619–3631.
[13] V. Mosorov, M. Zych, R. Hanus, D. Sankowski, A. Saoud, Improvement of Flow Velocity Measurement Algorithms Based on Correlation Function and Twin Plane Electrical Capacitance Tomography, Sensors 20 (1), 306.
[14] C.M. Salgado, L.E.B. Brandão, C.C. Conti, W.L. Salgado, Density prediction for petroleum and derivatives by gamma-ray attenuation and artificial neural networks, Appl. Radiat. Isot. 116 (2016) 143–149.
[15] Y. Tingting, W. Junqian, W. Lintai, X. Yong, Three-stage network for age estimation, CAAI Transactions on Intelligence Technology 4 (2019) 122–126.
[16] R. Ding, L. Dai, G. Li, H. Liu, TDD-net: a tiny defect detection network for printed circuit boards, CAAI Transactions on Intelligence Technology 4 (2019) 110–116.
[17] M. Roshani, M.A. Sattari, P.J.M. Ali, et al, X-ray tube with artificial neural network model as a promising alternative for radioisotope source in radiation based two phase flowmeters, Appl. Radiat. Isot. 164 (2020) 109255.
[18] M. Roshani, G. Phan, R.H. Faraj, et al, Proposing a gamma radiation based intelligent system for simultaneous analyzing and detecting type and amount of petroleum by-products. Nuclear, Eng. Technol. (2020).
[19] S. Goswami, H.J. Pant, D. Poswal, J.S. Samantray, S.R. Asolekar, Investigation of flow dynamics of wastewater in a pilot-scale constructed wetland using radiotracer technique, Appl. Radiat. Isot. 147 (2019) 70–75.
[20] R. Hanus, M. Zych, M. Kusy, M. Jaszczur, L. Petryka, Identification of liquid-gas flow regime in a pipeline using gamma-ray absorption technique and computational intelligence methods, Flow Meas. Instrum. 60 (2018) 17–23.
[21] J. Biswal, H.J. Pant, S. Goswami, J.S. Samantray, V.K. Sharma, K.S.S. Sarma, Measurement of flow rates of water in large diameter pipelines using radiotracer dilution method, Flow Meas. Instrum. 59 (2018) 194–200.
[22] E. Nazemi, S.A.H. Feghhi, G.H. Roshani, Void fraction prediction in two-phase flows independent of the liquid phase density changes, Radiat. Meas. 68 (2014) 49–54.
[23] G.H. Roshani, S.A.H. Feghhi, S. Setayeshi, Dual-modality and dual-energy gamma ray densitometry of petroleum products using an artificial neural network, Radiat. Meas. 82 (2015) 154–162.
[24] S. Abdul-Majid, Determination of wax deposition and corrosion in pipelines by neutron back diffusion collimation and neutron capture gamma rays, Appl. Radiat. Isot. 74 (2013) 102–108.
[25] D.F. Oliveira, J.R. Nascimento, C.A. Marinho, R.T. Lopes, Gamma transmission system for detection of scale in oil exploration pipelines, Nucl. Instrum. Methods Phys. Res., Sect. A 784 (2015) 616–620.
[26] T.P. Teixeira, C.M. Salgado, R.S.D.F. Dam, W.L. Salgado, Inorganic scale thickness prediction in oil pipelines by gamma-ray attenuation and artificial neural network, Appl. Radiat. Isot. 141 (2018) 44–50.
[27] W.L. Salgado, R.S.D.F. Dam, T.P. Teixeira, C.C. Conti, C.M. Salgado, Application of artificial intelligence in scale thickness prediction on offshore petroleum using a gamma-ray densitometer, Radiat. Phys. Chem. 168 (2020) 108549.
[28] J.P. Candeias, D.F. De Oliveira, M.J. Dos Anjos, R.T. Lopes, Scale analysis using X-ray microfluorescence and computed radiography, Radiat. Phys. Chem. 95 (2014) 408–411.
[29] D.F. Oliveira, R.S. Santos, A.S. Machado, A.S. Silva, M.J. Anjos, R.T. Lopes, Characterization of scale deposition in oil pipelines through X-Ray Microfluorescence and X-Ray microtomography, Appl. Radiat. Isot. 151 (2019) 247–255.
[30] D.B. Pelowitz, MCNP-X TM User's Manual, Version 2.5.0. LA-CP-05e0369. Los Alamos National, Laboratory (2005).
[31] E. Nazemi, G.H. Roshani, S.A.H. Feghhi, S. Setayeshi, R. Gholipour Peyvandi, A radiation-based hydrocarbon two-phase flow meter for estimating of phase fraction independent of liquid phase density in stratified regime, Flow Measurement and Instrumentations 46 (2015) 25–32.
[32] M.S. Mushtaq, A.H. Mellouk, Methodologies for Subjective Video Streaming QoE Assessment, Quality of Experience Paradigm in Multimedia Services (2017) 27–57.
[33] V. Vapnik, Statistical learning theory, Wiley, New York, 1998.
[34] N. Cristianini, J. Shawe-Taylor, An introduction to support vector machines, Cambridge University Press, Cambridge, 2000.
[35] K. Veropoulos , C. Campbell, N. Cristianini, Controlling the sensitivity of support vector machines. In: Proceedings of the international joint conference on artificial intelligence, Stockholm, Sweden, IJCAI99, workshop ML3 (1999) 55–60.
[36] I. Mukherjee, S. Routroy, Comparing the performance of neural networks developed by using Levenberg–Marquardt and Quasi-Newton with the gradient descent algorithm for modelling a multiple response grinding process, Expert Syst. Appl. 39 (2012) 2397–2407.